RSC Advances

PAPER

View Article Online
View Journal | View Issue

Cite this: *RSC Adv.*, 2020, **10**, 5734

Factors governing the competition between group IA and IB cations for monensin A: a DFT/PCM study

Todor Dudev,*[a] Diana Cheshmedzhieva,[a] Radoslava Dimitrova,[b] Peter Dorkov[c] and Ivayla Pantcheva*[b]

Received 22nd November 2019
Accepted 29th January 2020

DOI: 10.1039/c9ra09784h

rsc.li/rsc-advances

The affinity of monensin A to bind monovalent metal cations was evaluated by means of density functional theory (DFT) combined with polarizable continuum model (PCM) computations. The effect of various factors on complex formation between the monensinate A anion and group IA and IB metal ions was assessed. Competition between Na^+ taken as a reference and monovalent metal cations was estimated using the Gibbs free energy for substituting the ligand-bound Na^+ with its rival ions in the process [M^+-solution] + [Mon^-Na^+] → [Mon^-M^+] + [Na^+-solution] (M^+ = Li^+, K^+, Rb^+, Cs^+, Cu^+, Ag^+ and Au^+). The calculations revealed that the decrease in size of the cations accompanied by an increase of their accepting ability enhances the metal selectivity towards ligand donor atoms. In the gas-phase the affinity of monensinate A decreases in the order $Cu^+ > Li^+ > Na^+ > Au^+ > Ag^+ > K^+ > Rb^+ > Cs^+$. The complex formation can be manipulated by changing the solvent used. The polyether ionophore selectively binds Na^+ ions in polar solvents but could become Li^+ or Cu^+-selective in low-polarity solvents.

Introduction

Monensic acid A (monensin A, MonH) belongs to the group of natural polyether ionophores (PI) – a class of highly active molecules with pronounced biological efficacy. They are polyether polyalcohol monocarboxylic acids varying in molecular weight from 700 to 1000 g mol^{-1}.[1–3] The carboxylic moiety is placed at the "head" of the polyether chain while at least one hydroxyl group is located at the "tail" of the molecule. Alkyl substituents bound to the polyether chain are oriented externally ensuring the overall lipophilic character of the ligands. Polyether oxygens are placed inward forming a hydrophilic cavity able to host water molecules or monovalent metal ions.

The structure of monensic acid monohydrate ($MonH \cdot H_2O$) and its complexes with monovalent metal cations [Mon^-M^+] (M^+ = Li^+, Na^+, K^+, Rb^+, Ag^+) has been evaluated by X-ray crystallography on single crystals.[4–11] Data revealed that monensin reacts as a carboxylate monoanion (Mon^-) and the metal cations are coordinated by six oxygens of various origin. No participation of carboxylate group in the internal sphere of the metal ions was observed. Complexation of M^+ ions leads to the formation of a pseudochelate structure secured by a number of "head-to-tail" hydrogen bonds.

By wrapping monovalent metal ions as overall neutral compounds, monensin is able to transfer them through the lipid membranes into the intracellular space where dissociation of cations occurs thus disturbing metal homeostasis. Changes in the gradients of physiologically essential metal ions such as K^+ and Ca^{2+} induce a cascade of energy-consuming processes which lead to ultimate cell death. Monensin A is used as coccidiostat against *Eimeria* spp. but also possesses antibacterial, antiviral and promising antitumor properties.[12–17] It was observed that inclusion of monovalent metal ions into the structure of the ligand influences it's *in vitro* and *in vivo* activity.[18–25]

The striking feature of PI is their selectivity towards monovalent metal cations despite similarities between all of them from structural point of view and biological mode of action. An extensive study on affinity of monensin A to bind monovalent metal cations was performed in protic and dipolar aprotic solvents, in heterogeneous systems (water-organic phase) as well as in model biomembranes.[26–40] Experimental data (cyclovoltammetry, microcalorimetry, potentiometry)[26–40] revealed that monensinate complexes of IA cations are very stable with sharp stability maximum for sodium complex [Mon^-Na^+]. The observed selectivity was explained in terms of cavity – cation-size dependence and negative charge of ligand anion, introducing direct electrostatic stabilization. Generally, affinity of monensinate A anion toward alkali metal ions in polar solvents decreases in the order of $Na^+ > K^+ > Rb^+ > Cs^+$ although variation was observed in some cases depending on the reaction phase/medium and metal cations studied.

Thus, Henderson *et al.*[26] reported affinity order of $Na^+ > K^+ \approx Li^+ > Rb^+ > Cs^+$ in membranes and liquid crystals, confirmed by

[a]*Laboratory of Computational Chemistry and Spectroscopy, Faculty of Chemistry and Pharmacy, "St. Kl. Ohridski" University of Sofia, 1, J. Bourchier Blvd., 1164 Sofia, Bulgaria. E-mail: ohtttd@chem.uni-sofia.bg; Tel: +359-2-8161323*

[b]*Laboratory of Biocoordination and Bioanalytical Chemistry, Faculty of Chemistry and Pharmacy, "St. Kl. Ohridski" University of Sofia, 1, J. Bourchier Blvd., 1164 Sofia, Bulgaria. E-mail: ipancheva@chem.uni-sofia.bg; Tel: +359 2 8161446*

[c]*Biovet Ltd., Research & Development Department, Peshtera, Bulgaria*

studies of Ashton and Stenrauf[27] in model transport systems ($Na^+ > K^+ > Li^+ > Rb^+$). A slightly different sequence was evaluated by Cornelius *et al.*[29] using biomembranes: $Na^+ > K^+ > Tl^+ > Rb^+ > Cs^+$. Hoogerheide and Popov[31] studied affinity of monensinate anion to bind monovalent metal ions in anhydrous methanol, and detected decreased selectivity of the ligand in the order $Ag^+ > Na^+ > Tl^+ > K^+ > Rb^+ > Cs^+ > Li^+$, whereas later Mimouni *et al.*[36] observed some inversion between particular pairs of ions in methanol and biphasic systems. Furthermore, Forbes *et al.*[41] studied the gas-phase behaviour of monensin A towards IA metal ions to assess the maximum stability of [Mon$^-$K$^+$] as compared to other monovalent metal cations.

Although a substantial body of information has been accumulated on the monensin chemistry/biochemistry, the key factors governing its metal affinity are still not well defined. Here, we endeavor to shed light on this issue by employing a combination of density functional theory (DFT) calculations and polarizable continuum model (PCM) computations. The free energies of complex formation between monensinate anion and group IA and IB metal cations are evaluated and the role of various factors on the process (metal ion radius, its charge accepting power, and dielectric properties of the medium) is assessed. Note that our aim is to evaluate reliable trends of changes in the thermodynamic quantities rather than reproducing their absolute values. The approach adopted has proven quite successful in deciphering the mechanism of metal affinity/selectivity in a number of chemical/biological systems such as cyclodextrins,[42] enzymes,[43] signaling proteins,[44] and ion channels.[45]

Methods

Reaction modeled

The competition between the group IA and IB cations and Na^+ (taken as a reference) in monensinate A can be expressed in terms of the Gibbs free energy for substituting the ligand-bound Na^+ with its rival cations:

$$[M^+\text{-solution}] + [Mon^-Na^+] \rightarrow [Mon^-M^+] + [Na^+\text{-solution}] \quad (1)$$

In reaction (1), [Mon$^-$M$^+$] and [M$^+$/Na$^+$-solution] (M$^+$ = Li$^+$, K$^+$, Rb$^+$, Cs$^+$, Cu$^+$, Ag$^+$ and Au$^+$) denote the metal cation bound to monensinate A anion and unbound outside the host polyether moiety, respectively. The reaction was modeled in various dielectric media ranging from low polarity solvents characterized with $\varepsilon \approx 2$ (cyclohexane) and 4 (diethyl ether) to highly polar solvents with $\varepsilon \approx 32$ (methanol) and 78 (water). The positive free energy for reaction (1) implies a Na^+-selective binding site whereas the negative value implies a M^+-selective one. Ranking the free energies evaluated by reaction (1) reflects the relative affinity of the metal cations for the host molecule.

DFT/PCM calculations

All calculations were performed using Gaussian 09 package of programs.[46] All the structures were fully optimized in the gas phase at the B3LYP/6-31+G(d,p) level of theory yielding the respective electronic energies, E_{elect} of the studied species. SDD basis set and effective core potential were used for heavier metal ions in the series such as Rb^+, Cs^+, Ag^+ and Au^+. This combination of method/basis set was chosen for the present calculations as it proved reliable in reproducing the experimental structural parameters of [Mon$^-$Na$^+$] complex used as reference in this work. The optimized geometry of [Mon$^-$Na$^+$] complex (Fig. 1) is compared with the one determined from X-ray diffraction.[9] The interatomic distances between the oxygen atoms in monensinate ion and the sodium cation as well as selected bond angles are given in Table 1. As can be seen from the data in Table 1, the structure obtained from DFT computations is very close to that determined by X-ray diffraction. The comparison between calculated structural parameters and available experimental data shows quantitative agreement between theory and experiment for the geometry of [Mon$^-$Na$^+$] complex (Table 1).

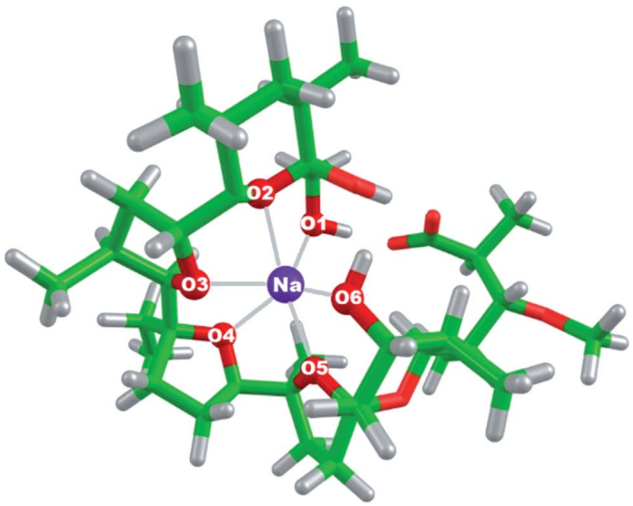

Fig. 1 Optimized geometry of [Mon$^-$Na$^+$] complex at the B3LYP/6-31+G(d,p) level of theory. Color scheme: C – green, O – red, H – light grey, Na – purple.

Table 1 Comparison between selected computed and experimental bond distances (Å) and bond angles (°) in [Mon$^-$Na$^+$] complex

Bond length/bond angle	[Mon$^-$Na$^+$]	
	Exp[9]	Calcd[a]
$Na–O_1$	2.34	2.34
$Na–O_2$	2.33	2.37
$Na–O_3$	2.60	2.60
$Na–O_4$	2.45	2.45
$Na–O_5$	2.41	2.46
$Na–O_6$	2.38	2.34
Na–O average	**2.42**	**2.42**
$O_1–Na–O_2$	68.2	68.6
$O_2–Na–O_5$	173.3	163.5
$O_1–Na–O_5$	117.3	122.8
$O_1–Na–O_6$	113.5	111.4
$O_5–Na–O_6$	76.2	75.5

[a] Optimization at the B3LYP/6-31+G(d,p) level of theory.

Table 2 Experimental and estimated solvation free energies (kcal mol^{-1}) employed in the calculations. Estimated ΔG^{s} are determined as a multiple of ΔG^{78} (exp) and $\Delta G^{\varepsilon}/\Delta G^{78}$ ratio from SMD calculations given on the left of the respective ΔG^{ε} (est) column

Metal ion	ΔG^{78} (exp)[50]	$\Delta G^{32}/\Delta G^{78}$ (calc)	ΔG^{32} (est)	$\Delta G^{4}/\Delta G^{78}$ (calc)	ΔG^{4} (est)	$\Delta G^{2}/\Delta G^{78}$ (calc)	ΔG^{2} (est)
Li^+	−123.5	0.974	−120.3	0.768	−94.8	0.560	−69.2
Na^+	−98.3	0.968	−95.2	0.763	−75.0	0.554	−54.5
K^+	−80.8	0.960	−77.5	0.757	−61.1	0.545	−44.0
Rb^+	−76.6	0.971	−74.4	0.766	−58.7	0.557	−42.7
Cs^+	−71.0	0.967	−68.7	0.764	54.2	0.554	−39.3
Cu^+	−148.7[a]	0.978	−145.4	0.770	−114.5	0.562	−83.5
Ag^+	−114.5	0.975	−111.6	0.768	−88.0	0.560	−64.1
Au^+	−124.8[b]	0.977	−121.9	0.768	−95.9	0.561	−70.0

[a] Estimated from the experimental solvation energy of Ag^+ and the respective ratio between the calculated ΔG^{s} of Cu^+ and Ag^+. [b] Estimated from the experimental solvation energy of Ag^+ and the respective ratio between the calculated ΔG^{s} of Au^+ and Ag^+.

Vibrational analysis was performed at the same level of theory. No imaginary frequency was found for any of the optimized structures indicating a local minimum of the potential energy surface. The vibrational frequencies were used to obtain the thermal energies, including the zero-point energy, E_T, and entropy, S. These values were employed in evaluating the gas-phase Gibbs free energies for reaction (2), ΔG^{1}, at room temperature, $T = 298.15$ K, according to (3):

$$[M^+] + [Mon^-Na^+] \rightarrow [Mon^-M^+] + [Na^+] \quad (2)$$

$$\Delta G^{1} = \Delta E_{elect} + \Delta E_T - T\Delta S, \quad (3)$$

where ΔE_{elect}, ΔE_T and ΔS are the respective differences between the products and reactants. Solvation effects were accounted for by employing polarizable continuum model calculations at SMD level[47] as implemented in Gaussian 09 suite of programs. Single point calculations of each geometrically optimized structure were performed in each solvent. The differences between the gas-phase and condensed-phase energies yielded the free energies of solvation, $\Delta G_{solv}{}^{\varepsilon}$, of the respective constructs. These were used in evaluating the reaction free energies in solution, ΔG^{ε}:

$$\Delta G^{\varepsilon} = \Delta G^{1} + \Delta G_{solv}{}^{\varepsilon}([Mon^-M^+]) + \Delta G_{solv}{}^{\varepsilon}([Na^+\text{-solution}]) - \Delta G_{solv}{}^{\varepsilon}([Mon^-Na^+]) - \Delta G_{solv}{}^{\varepsilon}([M^+\text{-solution}]) \quad (4)$$

Notably, the experimentally determined solvation free energies for the metal cations in aqueous solution (where available) were used in the calculations. For other cations and solvents estimated values were employed where the dependencies in the theoretically evaluated quantities in combination with the experimental values were used to determine the respective $\Delta G_{solv}{}^{\varepsilon}([M^+/Na^+\text{-solution}])$ (Table 2). Such a methodology (employing thermodynamic cycle with experimental solvation free energies of some species) has proven quite accurate in reproducing the experimental thermodynamic data.[48]

The basis set superposition error for the type of exchange reactions modeled by reaction (1) was found to be insignificant[49] and was thus not considered in the present calculations.

Results and discussion

Group IA

Alkali metals form spherical monovalent cations whose ionic radius gradually increases with increasing the atomic number (Table 3). The ion charge density decreases in the same direction thus weakening the ligand affinity of the metal and rendering the bulkiest Cs^+ the weakest Lewis' acid (with lowest ligand affinity) in the group.

Structures of the fully optimized metal complexes with monensinate A anion are given in Fig. 2. The metal cation binds

Table 3 Structural and electronic characteristics of group IA and IB metal cations with coordination number of 6

Metal ion	Ionic radius[51] (Å)	Average M–O distance in $[Mon^-M^+]$ (Å)	Charge transfer to the metal (e) in M^+–(CH_3OCH_3)[a,b]	Charge transfer to the metal (e) in M^+–(CH_3OH)[a,c]
Li^+	0.76 (VI)	2.26	0.286	0.260
Na^+	1.02 (VI)	2.42	0.215	0.198
K^+	1.38 (VI)	2.81	0.166	0.152
Rb^+	1.52 (VI)	2.89	0.142	0.132
Cs^+	1.67 (VI)	3.08	0.129	0.119
Cu^+	0.77 (VI)	2.44	0.360	0.338
Ag^+	1.15 (VI)	2.56	0.300	0.281
Au^+	1.37 (VI)	2.71	0.412	0.381

[a] This work. Calculated from the Hirshfeld population analysis at the B3LYP/6-31+G(d,p) level. [b] CH_3OCH_3 is used as a model for the ether group in monensin A. [c] CH_3OH is used as a model for the hydroxyl moiety in monensin A.

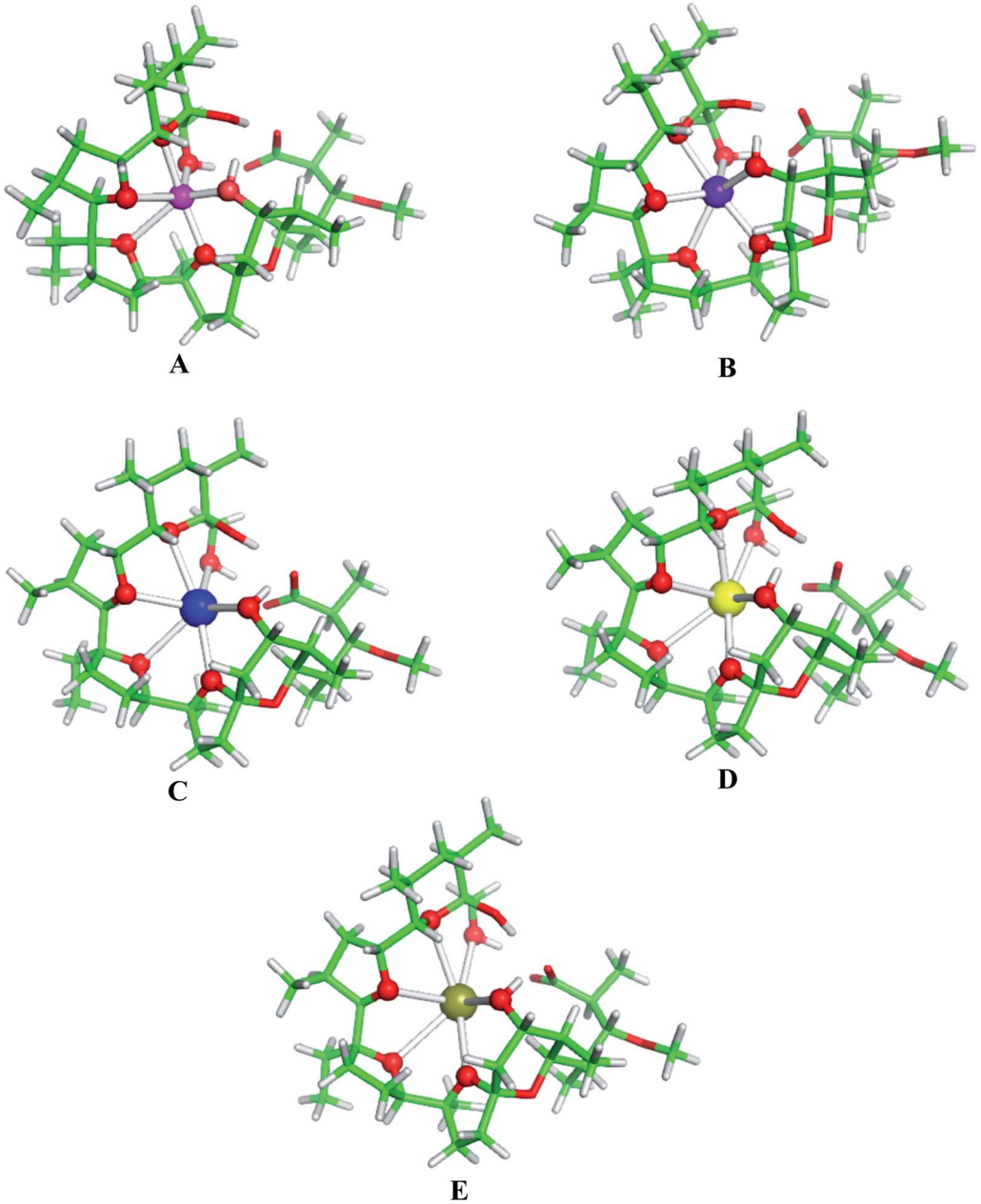

Fig. 2 B3LYP/6-31+G(d,p) fully optimized structures of monensinate A anion bound to (A) Li^+, (B) Na^+, (C) K^+, (D) Rb^+ and (E) Cs^+. Color scheme: C – green, O – red, H – light grey, Li – magenta, Na – purple, K – blue, Rb – yellow, Cs – deep olive.

to ether and hydroxyl oxygens. The metal coordination numbers are 6 in agreement with the experimental observations.[4–6,8–12] The average M^+–O bond length increases in the same direction (spanning the range of 2.28–3.08 Å) which is compatible with the increased ionic radius of the metal species (Table 3). This result implies that the monensinate A ligand is relatively flexible and its internal cavity, unlike that of other "rigid" macrocycles (*e.g.* crown ethers), can fluctuate in size adapting to the spatial requirements of the guest cation.

The outcome of the metal ion competition in solution (reaction (1)) is a balance between electronic and solvation effects. The role of the former can be assessed by following the trends of changes in the gas-phase free energies, ΔG^1. As the data in Table 4 indicate, ΔG^1 changes in agreement with the affinity of the metal cation for the ligands (measured as the amount of the charge transferred from the ligand to the metal; the greater the charge accepted, the higher the metal affinity; Table 3). It is the greatest for Li^+ ions and gradually attenuates in going down the group. Accordingly, ΔG^1 increases from the Li^+ to Cs^+/Na^+ substitution. Thus, the electronic effects align the affinity of the metal cations for monensinate A anion as $Li^+ > Na^+ > K^+ > Rb^+ > Cs^+$.

The solvation effects, however, affect the affinity order: while it remains the same in low-polarity solvents (with dielectric

Table 4 Gibbs free energies of $M^+ \rightarrow Na^+$ metal exchange, ΔG^{ε}, for reaction (1) evaluated for media with varying dielectric constant ε[a]

Reaction	ΔG^{ε} (kcal mol^{-1})
[Li^+-solution] + [Mon^-Na^+] → [Mon^-Li^+] + [Na^+-solution]	$\Delta G^1 = -20.5$
	$\Delta G^2 = -5.4$
	$\Delta G^4 = 0.0$
	$\Delta G^{32} = 5.7$
	$\Delta G^{78} = 5.9$
[K^+-solution] + [Mon^-Na^+] → [Mon^-K^+] + [Na^+-solution]	$\Delta G^1 = 27.2$
	$\Delta G^2 = 17.4$
	$\Delta G^4 = 14.0$
	$\Delta G^{32} = 9.2$
	$\Delta G^{78} = 9.3$
[Rb^+-solution] + [Mon^-Na^+] → [Mon^-Rb^+] + [Na^+-solution]	$\Delta G^1 = 61.7$
	$\Delta G^2 = 49.4$
	$\Delta G^4 = 44.7$
	$\Delta G^{32} = 36.8$
	$\Delta G^{78} = 35.4$
[Cs^+-solution] + [Mon^-Na^+] → [Mon^-Cs^+] + [Na^+-solution]	$\Delta G^1 = 76.2$
	$\Delta G^2 = 60.7$
	$\Delta G^4 = 54.3$
	$\Delta G^{32} = 45.3$
	$\Delta G^{78} = 43.6$
[Cu^+-solution] + [Mon^-Na^+] → [Mon^-Cu^+] + [Na^+-solution]	$\Delta G^1 = -31.6$
	$\Delta G^2 = -2.0$
	$\Delta G^4 = 8.7$
	$\Delta G^{32} = 15.0$
	$\Delta G^{78} = 14.9$
[Ag^+-solution] + [Mon^-Na^+] → [Mon^-Ag^+] + [Na^+-solution]	$\Delta G^1 = 13.5$
	$\Delta G^2 = 23.1$
	$\Delta G^4 = 26.4$
	$\Delta G^{32} = 28.7$
	$\Delta G^{78} = 28.3$
[Au^+-solution] + [Mon^-Na^+] → [Mon^-Au^+] + [Na^+-solution]	$\Delta G^1 = 2.4$
	$\Delta G^2 = 18.4$
	$\Delta G^4 = 24.1$
	$\Delta G^{32} = 27.3$
	$\Delta G^{78} = 26.6$

[a] In assessing the relative metal affinities, the affinity of the reference metal cation (Na^+) is taken as 0, whereas that for the rest of the metal cations follows the trends in ΔG^{ε}.

constant 2–4), it changes in polar solvents (methanol and water). The respective ΔG^{32} and ΔG^{78} for Li^+/Na^+ exchange, due to the high desolvation penalty of Li^+ (left-hand side of reaction (1) and Table 2), become positive. The free energies in polar solvents for the rest of the metals decrease but remain on a positive ground. Thus, the affinity series in polar solvents (methanol for example) becomes $Na^+ > Li^+ > K^+ > Rb^+ > Cs^+$. This is in good agreement with the experimental results indicating that monensinate A is selective for Na^+ in polar solvents among the group IA cations.[31,36]

Group IB

The physico-chemical properties of the coinage metal cations (Cu^+, Ag^+ and Au^+), as compared to those of the respective alkali metal ions, are strongly influenced by the presence of d orbitals in the outer electron shell, which by hybridizing with the valence s orbitals lower their energy thus reducing the ionic radius and enhancing their charge accepting ability. Indeed, as the data in Table 3 (last two columns) indicate, the charge transfer from the ligands donor groups to the group IB metal cations is greater (meaning higher affinity) than that to the respective alkali metal ions from the same period. Furthermore, the Wiberg indices[52], evaluated from the NBO population analysis revealed that the bonds between the group IB metals and ligating oxygen atoms from monensin A are stronger than those of the respective IA metal–oxygen counterparts: the mean Wiberg indices for the Cu^+–O, Ag^+–O and Au^+–O bonds are 0.0578, 0.0601 and 0.0917 a.u., respectively, whereas those for the Li^+–O, Na^+–O, K^+–O, Rb^+–O and Cs^+–O bonds are 0.0159, 0.0135, 0.0157, 0.0063 and 0.0104 a.u., respectively.

The structures of fully optimized complexes of monensin A with Cu^+, Ag^+ and Au^+ are presented in Fig. 3. In all the structures, the metal cation is coordinated to six oxygen atoms.[7] The smaller ionic radii of the coinage metal ions are compatible with shorter M^+–O distances in monensinate A complexes relative to their alkali metal counterparts (Table 3). The gas-phase $M^+ \rightarrow Na^+$ substitution energies for Cu^+, Ag^+ and Au^+ are much more favorable than those of the respective group IA metals from the same period (K^+, Rb^+ and Cs^+, respectively; Table 4). The affinity order for the entire group I in the gas phase reads $Cu^+ > Li^+ > Na^+ > Au^+ > Ag^+ > K^+ > Rb^+ > Cs^+$.

In low polarity solvents (for example $\varepsilon \approx 2$) this order changes in favor of Li^+: $Li^+ > Cu^+ > Na^+ > K^+ > Au^+ > Ag^+ > Rb^+ > Cs^+$. The sequence changes again in polar solvents (methanol), this time in favor of Na^+: $Na^+ > Li^+ > K^+ > Cu^+ > Au^+ > Ag^+ > Rb^+ > Cs^+$. Note that the coinage metal ions, although possessing higher affinity to the ligand than the respective alkali metal cations, are relegated to lower positions in the solution affinity scale due to the high desolvation penalty to be paid in condensed phase (reaction (1) and Table 2).

Concluding remarks

The calculations performed reveal the following key determinants of the monovalent metal selectivity in monensinate A anion:

- The metal ion radius: smaller size cations, with higher positive charge density, are more competitive than their bulkier counterparts;

- The metal cation charge accepting ability: increasing the metal charge accepting ability, especially for d-elements, which translates into increased affinity toward the surrounding ligands (donor atoms), enhances the metal ion selectivity;

- The dielectric properties of the medium: low-polarity solvents favor the smaller ions possessing high ligand affinity (Li^+ and Cu^+); in polar solvents, characterized with high dielectric constants, the competitiveness of the medium-size cations, particularly Na^+, increases.

The size of the internal cavity appears to be a secondary factor of the metal selectivity as the pore is relatively flexible and adaptable to certain extent to the spatial requirements of the incoming metal cations.

Note that the role of the solvent in governing the metal affinity of monensinate A anion is evaluated for the first time here (to the best of our knowledge). Our results imply that the metal selectivity of monensin A can be manipulated by

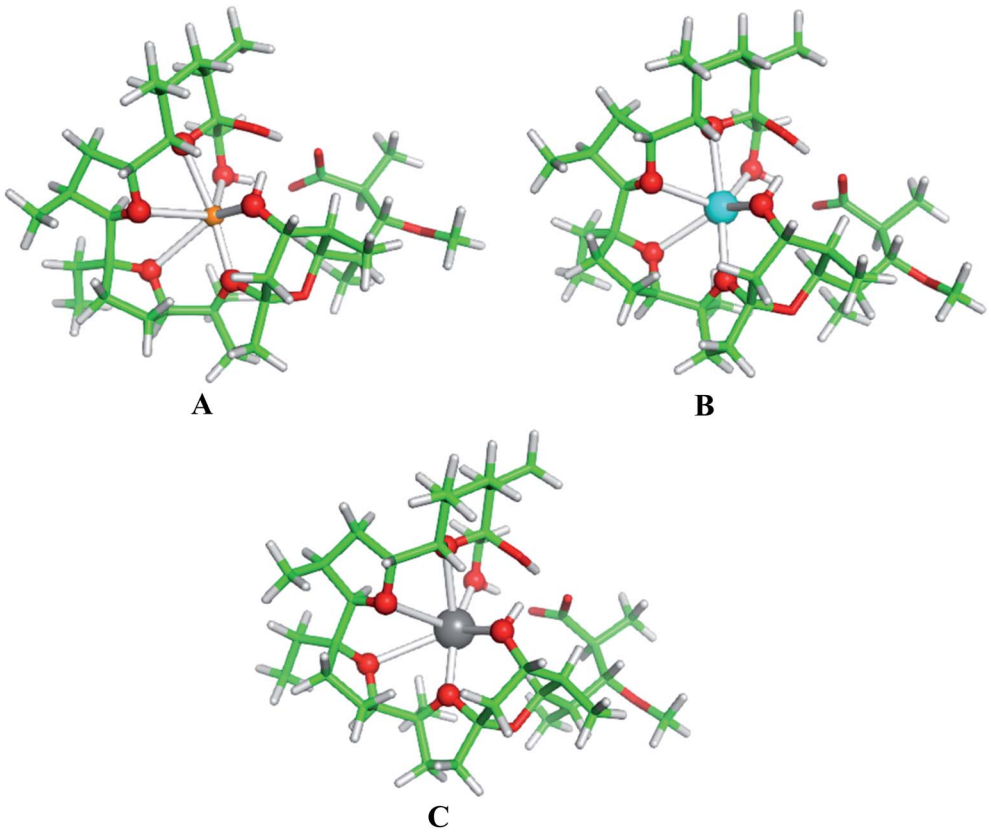

Fig. 3 B3LYP/6-31+G(d,p) fully optimized structures of monensinate A bound to (A) Cu^+, (B) Ag^+ and (C) Au^+. Color scheme: C – green, O – red, H – light grey, Cu – orange, Ag – cyan, Au – grey.

changing the solvent used: the polyether host selectively binds Na^+ in polar solvents (methanol and water) but could become Li^+ or Cu^+-selective in low-polarity solvents such as alkyl ethers, hydrocarbons and their halogenated derivatives.

Conflicts of interest

There are no conflicts to declare.

Acknowledgements

The authors are thankful for the support by National Science Fund, Bulgarian Ministry of Education and Science (contract no. KP-06-H29/3).

References

1 A. Agtarap, J. W. Chamberlin, M. Pinkerton and L. K. Steinrauf, Structure of monensic acid, a new biologically active compound, *J. Am. Chem. Soc.*, 1967, **89**, 5737–5739.

2 L. K. Steinrauf, M. Pinkerton and J. W. Chamberlin, The structure of nigericin, *Biochem. Biophys. Res. Commun.*, 1968, **33**, 29–31.

3 M. Mitani, T. Yamanishi and Y. Miyazaki, Salinomycin: a new monovalent cation ionophore, *Biochem. Biophys. Res. Commun.*, 1975, **66**, 1231–1236.

4 M. Pinkerton and L. K. Stenrauf, Molecular structure of monovalent metal cation complexes of monensin, *J. Mol. Biol.*, 1970, **49**, 533–546.

5 W. K. Lutz, F. K. Winkler and J. D. Dunitz, Crystal structure of the antibiotic monensin. Similarities and differences between free acid and metal complex, *Helv. Chim. Acta*, 1971, **54**, 1103–1108.

6 W. L. Duax, G. D. Smith and P. D. Strong, Complexation of metal ions by monensin. Crystal and molecular structure of hydrated and anhydrous crystal forms of sodium monensin, *J. Am. Chem. Soc.*, 1980, **102**, 6725–6729.

7 D. M. Walba, M. Hermsmeier, R. C. Haltiwanger and J. H. Noordik, Crystal structures of monensin B lithium and silver salts, *J. Org. Chem.*, 1986, **51**, 245–247.

8 W. Pangborn, W. Duax and D. Langs, The hydrated potassium complex of the ionophore monensin A, *J. Am. Chem. Soc.*, 1987, **109**, 2163–2165.

9 A. Huczynski, M. Ratajczak-Sitarz, A. Katrusiak and B. Brzezinski, Molecular structure of the 1:1 inclusion complex of monensin A sodium salt with acetonitrile, *J. Mol. Struct.*, 2007, **832**, 84–89.

10 A. Huczynski, M. Ratajczak-Sitarz, A. Katrusiak and B. Brzezinski, Molecular structure of the 1:1 inclusion

complex of monensin A lithium salt with acetonitrile, *J. Mol. Struct.*, 2007, **871**, 92–97.

11 A. Huczynski, M. Ratajczak-Sitarz, A. Katrusiak and B. Brzezinski, Molecular structure of rubidium six-coordinated dihydrate complex with monensin A, *J. Mol. Struct.*, 2008, **883**, 224–229.

12 P. Butaye, L. A. Devriese and F. Haesebrouck, Antimicrobial growth promoters used in animal feed: effects of less well known antibiotics on gram-positive bacteria, *Clin. Microbiol. Rev.*, 2003, **16**, 175–188.

13 D. A. Kevin II, D. A. F. Meujo and M. T. Hamann, Polyether ionophores: broad-spectrum and promising biologically active molecules for the control of drug-resistant bacteria and parasites, *Expert Opin. Drug Discovery*, 2009, **4**, 109–146.

14 H. D. Chapman, T. K. Jeffers and R. B. Williams, Forty years of monensin for the control of coccidiosis in poultry, *Poult. Sci.*, 2010, **89**, 1788–1801.

15 V. Rajendran, H. S. Ilamathi, S. Dutt, T. S. Lakshminarayana and P. C. Ghosh, Chemotherapeutic potential of monensin as an antimicrobial agent, *Curr. Top. Med. Chem.*, 2018, **18**, 1976–1986.

16 A. Huczyński, G. Klejborowska, M. Antoszczak, E. Maj and J. Wietrzyk, Anti-proliferative activity of monensin and its tertiary amide derivatives, *Bioorg. Med. Chem. Lett.*, 2015, **25**, 4539–4543.

17 V. Kaushik, J. S. Yakisich, A. Kumar, N. Azad and A. K. V. Iyer, Ionophores: potential use as anticancer drugs and chemosensitizers, *Cancers*, 2018, **10**, 360.

18 D. Carriere, P. Casellas, G. Richer, P. Gros and F. K. Jansen, Endocytosis of an antibody ricin A-chain conjugate (immuno-A-toxin) adsorbed on colloidal gold. Effects of ammonium chloride and monensin, *Exp. Cell Res.*, 1985, **156**, 327–340.

19 E. V. Wattenberg, P. L. McNeil, H. Fujiki and M. R. Rosner, Palytoxin down-modulates the epidermal growth factor receptor through a sodium-dependent pathway, *J. Biol. Chem.*, 1989, **264**, 213–219.

20 W. T. Shier and D. J. DuBourdieu, Sodium- and calcium-de-endent steps in the mechanism of neonatal rat cardiac myocyte killing by lonophores. I. The sodium-carrying lonophore, monensin, *Toxicol. Appl. Pharmacol.*, 1992, **116**, 38–46.

21 N. R. Bury, M. Grosell, A. K. Grover and C. M. Wood, ATP-dependent silver transport across the basolateral membrane of rainbow trout gills, *Toxicol. Appl. Pharmacol.*, 1999, **159**, 1–8.

22 C. C. Häse, N. D. Fedorova, M. Y. Galperin and P. A. Dibrov, Sodium ion cycle in bacterial pathogens: evidence from cross-genome comparisons, *Microbiol. Mol. Biol. Rev.*, 2001, **65**, 353–370.

23 W. Li, B. Dasgeb, T. Phillips, Y. Li, M. Chen, W. Garner and D. T. Woodley, Wound-Healing Perspectives, *Dermatol. Clin.*, 2005, **23**, 181–192.

24 D. Łowicki, A. Huczyński, J. Stefańska and B. Brzezinski, Syntheses, structural and antimicrobial studies of a new N-allylamide of monensin A and its complexes with monovalent metal cations, *Tetrahedron*, 2009, **65**, 7730–7740.

25 D. Łowicki, A. Huczyński, J. Stefańska and B. Brzezinski, Structural characterization and antibacterial activity against clinical isolates of Staphylococcus of N-phenylamide of monensin A and its 1:1 complexes with monovalent cations, *Eur. J. Med. Chem.*, 2010, **45**, 4050–4057.

26 P. J. Henderson, J. D. McGiven and J. B. Chappell, The action of certain antibiotics on mitochondrial, erythrocyte and artificial phospholipid membranes. The role of induced proton permeability, *Biochem. J.*, 1969, **111**, 521–535.

27 R. Ashton and L. K. Stenrauf, Thermodynamic consideration of the ion transporting antibiotics, *J. Mol. Biol.*, 1970, **49**, 547–556.

28 W. K. Lutz, P. U. Früh and W. Simon, Microcalorimetric determination of ΔH^0, ΔG^0 and ΔS^0 for the interaction of the carrier antibiotics nigericin and monensin with sodium and potassium ions, *Helv. Chim. Acta*, 1971, **54**, 2767–2770.

29 G. Cornelius, W. Gartner and D. H. Haynes, Cation complexation by valinomycin- and nigericin-type ionophores registered by the fluorescence signal of Tl^+, *Biochemistry*, 1974, **13**, 3052–3057.

30 P. G. Gertenbach and A. I. Popov, Solution chemistry of monensin and its alkali metal ion complexes. Potentiometric and spectroscopic studies, *J. Am. Chem. Soc.*, 1975, **97**, 4738–4744.

31 J. G. Hoogerheide and A. I. Popov, Study of monensin complexes with monovalent metal ions in anhydrous methanol solutions, *J. Solution Chem.*, 1978, **7**, 357–372.

32 J. G. Hoogerheide and A. I. Popov, A study of metal complexes of a naturally occurring macrocyclic ionophore – monensin, *J. Solution Chem.*, 1979, **8**, 83–95.

33 B. Cox, N. van Truong, J. Rzeszotarska and H. Schneider, Stability constants of complexes of monensin and lasalocid with alkali-metal and alkaline-earth-metal ions in protic and polar aprotic solvents, *J. Chem. Soc., Faraday Trans. 1*, 1984, **80**, 3275–3284.

34 B. G. Cox, N. van Truong, J. Rzeszotarska and H. Schneider, Rates and equilibria of alkali metal and silver ion complex formation with monensin in ethanol, *J. Am. Chem. Soc.*, 1984, **106**, 5965–5969.

35 M. Hebrant, Y. Pointud and J. Juillard, Thermodynamics of reaction in heterogeneous systems (water-organic phases) between the ionophore monensin and alkali metal cations, *J. Phys. Chem.*, 1991, **95**, 3653–3662.

36 M. Mimouni, S. Perrier, Y. Pointud and J. Juillard, Selectivity of bacterial ionophore monensin for monovalent metal cations. Solvent effects in methanol and biphasic water-organic systems, *J. Solution Chem.*, 1993, **22**, 769–785.

37 S. Filipek, J. Rzeszotarska and M. K. Kalinowski, Polarographic Study of Tl^+, Li^+, Na^+ K^+ and Cs^+ complexes with monensin anion in dipolar aprotic solvents, *Monatsh. Chem.*, 1994, **125**, 801–809.

38 Y. Pointud, C. Bernard, S. Touzain, L. Astier, B. Sabatier and J. Juillard, Thermodynamics of complexation of monovalent

metal cations by the ionophore monensin free acid in acetonitrile, *J. Solution Chem.*, 1997, **26**, 479–495.

39 E. Wagner-Czauderna, J. Rzeszotarska, E. Orlowska and M. K. Kalinowski, Complexing ability of monensin anion for alkali metal cations in binary mixtures of dipolar aprotic solvents, *Ber. Bunsenges. Phys. Chem.*, 1997, **101**, 1154–1157.

40 N. Ben-Tal, D. Sitkoff, S. Bransburg-Zabary, E. Nachliel and M. Gutman, Theoretical calculations of the permeability of monensin cation complexes in model bio-membranes, *Biochim. Biophys. Acta*, 2000, **1466**, 221–233.

41 M. W. Forbes, D. A. Volmer, G. J. Francis and D. K. Böhme, A comparison of data analysis methods for determining gas phase stabilities by CID: alkali metal complexes of polyether ionophore antibiotics, *J. Am. Soc. Mass Spectrom.*, 2005, **16**, 779–791.

42 S. E. Angelova, V. K. Nikolova and T. M. Dudev, Determinants of the host-guest interactions between α-, β- and γ-cyclodextrins and group IA, IIA and IIIA metal cations: a DFT/PCM study, *Phys. Chem. Chem. Phys.*, 2017, **19**, 15129–15136.

43 T. Dudev, D. Cheshmedzhieva and L. Doudeva, Competition between abiogenic Al^{3+} and native Mg^{2+}, Fe^{2+} and Zn^{2+} ions in protein binding sites: implications for aluminum toxicity, *J. Mol. Model.*, 2018, **24**, 55.

44 T. Dudev, C. Grauffel and C. Lim, How Pb^{2+} binds and modulates properties of Ca^{2+}-signaling proteins, *Inorg. Chem.*, 2018, **57**, 14798–14809.

45 T. Dudev and C. Lim, Ion selectivity strategies of sodium channel selectivity filters, *Acc. Chem. Res.*, 2014, **47**, 3580–3587.

46 M. J. Frisch, G. W. Trucks, H. B. Schlegel, G. E. Scuseria, M. A. Robb, J. R. Cheeseman, J. A. Montgomery Jr, T. Vreven, K. N. Kudin, J. C. Burant, J. M. Millam, S. S. Iyengar, J. Tomasi, V. Barone, B. Mennucci, M. Cossi and G. Scalmani, *et al.*, *Gaussian 09*, Gaussian Inc., 2009.

47 A. V. Marenich, C. J. Cramer and D. G. Truhlar, Universal solvation model based on solute electron density and on a continuum model of the solvent defined by the bulk dielectric constant and atomic surface tensions, *J. Phys. Chem. B*, 2009, **113**, 6378–6396.

48 N. Kircheva and T. Dudev, Novel insights into gallium's mechanism of therapeutic action: a DFT/PCM study of the interaction between Ga^{3+} and ribonucleotide reductase substrates, *J. Phys. Chem. B*, 2019, **123**, 5444–5451.

49 T. Dudev and C. Lim, Determinants of K^+ vs Na^+ selectivity in potassium channels, *J. Am. Chem. Soc.*, 2009, **131**, 8092–8101.

50 H. L. Friedman and C. V. Krishnan, in *Water: A Comprehensive Treatise*, ed. F. Franks, Plenum Press, New York, 1973, vol. 3, pp. 1–118.

51 R. D. Shannon, Revised effective ionic radii and systematic studies in interatomic distances in halides and chalcogenides, *Acta Crystallogr., Sect. A: Found. Crystallogr.*, 1976, **32**, 751–767.

52 K. B. Wiberg, Application of the pople-santry-segal CNDO method to the cyclopropylcarbinyl and cyclobutyl cation and to bicyclobutane, *Tetrahedron*, 1968, **24**, 1083–1096.